

First arriving signals in layered waveguides.

An approach based on dispersion diagrams

A. V. Shanin

M.V.Lomonosov Moscow State University, department of physics

119992, Russia, Moscow, Leninskie gory, MSU

July 15, 2021

Abstract

The first arriving signal (FAS) in a layered waveguide is investigated. It is well known that the velocity of such a signal is close to the velocity of the fastest medium in the waveguide, and it may be bigger than the fastest group velocity given by the dispersion diagram of the waveguide. Usually the FAS pulse decays with the propagation distance. A model layered waveguide is studied in the paper. It is shown that the FAS is associated with the pseudo-branch structure of the dispersion diagram. The velocity of FAS is determined by the slope of the pseudo-branch. The decay is exponential and it depends on the structure of the pseudo-branch.

1 Introduction

Consider a layered 2D acoustic waveguide, which is homogenous in the x -direction and has a sandwich structure in the y -direction. The media constituting the waveguide can be elastic, liquid or gaseous. Waves in such a waveguide are described by a dispersion diagram in the (ω, k) coordinates (ω is the temporal circular frequency, k is the wavenumber in the x -direction). Usually the dispersion diagram is a graph consisting of several branches (curves). Each point of the dispersion diagram is characterized by two important parameters, namely by phase velocity $v_p = \omega/k$ and group velocity $v_g = (dk/d\omega)^{-1}$ (the derivative $dk/d\omega$ is the slope of corresponding branch of the dispersion diagram). It is well known that wave pulses propagate in the waveguide with corresponding group velocities.

It is well known also that in the experiment typically one can observe the *first arriving signal* (FAS) propagating with the velocity of the fastest medium in the structure of the waveguide. In the case of a single elastic isotropic medium the velocity of the FAS is close to the velocity of the longitudinal waves. In some cases the velocity of the FAS is bigger than any of the group velocities provided by the dispersion diagram. The FAS pulse decays with propagation distance unlike the pulses corresponding to usual modal pulses (the latter are called *guided waves* in the medical-related literature). Thus, FAS is a transient process in a waveguide. It can negligibly small very far from the source, however at moderate distances it can be an important

phenomenon.

The most known applications of FAS are related to medical acoustics (see e.g. [1, 2]). A long bone can be considered as a tubular waveguide constituted of three media: a thin outer layer of dense (cortical) bone, a sponge bone underneath, and a liquid marrow core in the center. The fastest wave that can theoretically propagate in such media (taken separately as infinite spaces) is the longitudinal wave in the cortical bone. The sponge bone and the marrow bear much slower waves. However, when a standard analysis of a waveguide is performed (say, by the finite element method) the dispersion diagram contains no branch having group velocity close to the longitudinal cortical velocity.

There exist different approaches to describe FAS. The most comprehensive approach has been proposed by Miklowitz and Randles in [3]. This approach considers an analytical continuation of the dispersion diagram. After passing some branch points, it is possible to find a single branch of the dispersion diagram whose group velocity and decay correspond to FAS. Another analytical approach is an application of the classical Cagniard–deHoop technique to invert the Fourier transform in the time domain [4]. An approximate approach to FAS is described in [5], where this type of waves is treated as a head wave. Also FAS can be approximately described as a leaky mode. For this, the slow media composing the waveguide are declared as elastic half-spaces, while the fastest medium remains to be a layer. Such an approach enables one to compute (at least in the simplest cases) the velocity

and the decay of FAS with an acceptable accuracy.

The aim of the current paper is to present a model of FAS based on an elementary analysis of real dispersion diagrams of a layered waveguide. It is known [6] that a wave process in a layered waveguide can be treated as an interaction between the modes of different types and velocities. Thus, the dispersion diagram has a “terrace-like” structure formed by overlapping of different sets of branches. Since typically no crossing of the branches can happen (except the branches corresponding to non-interacting waves), there occur quasi-crossings at which the type of the mode is changing. A typical fragment of a dispersion diagram is shown in Fig. 1 (this is a dispersion diagram of a model two-media acoustic waveguide studied in the paper). The visible line of the smallest slope (although this line can be composed of segments corresponding to different branches) is a *pseudo-branch*) relating to the FAS.

In the current paper this idea is developed into an analytical model. An approximation of a fragment of the dispersion diagram by a sum of a tangent function and a linear function is constructed. An analytical continuation of the approximation to the domain of positive $\text{Im}[\omega]$ is performed. The tangent function tends to an imaginary constant there. Using this trick, the estimation of the decay of FAS is obtained.

The idea to study the analytical continuation of the dispersion diagram is inspired by the Miklowitz–Randles method [3]. In the paper we briefly describe this method and its connection with the description of the FAS as

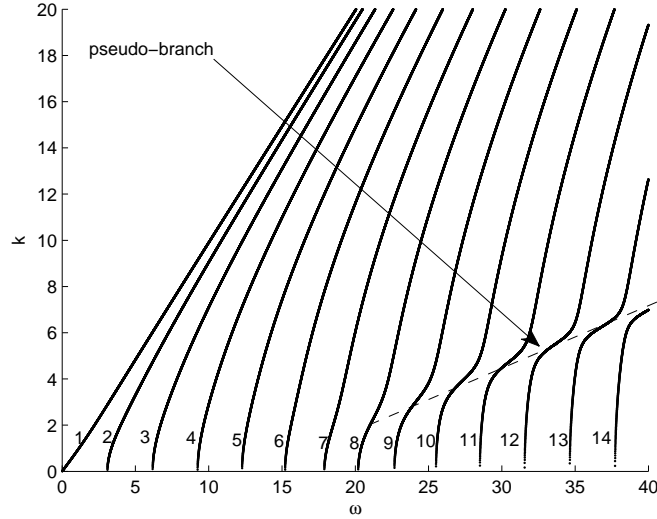


Fig. 1: A dispersion diagram of the waveguide composed of two layers
a leaky wave.

The structure of the paper is as follows. In Section II a sample problem is formulated. In Section III a numerical modeling of pulse propagation in the two-media problem is performed. The presence of FAS and its exponential decay are established. In Section IV the approach by Miklowitz–Randles is applied to the waveguide. The branch of the dispersion diagram responsible for FAS is found. In Section V the properties of FAS are compared to those of a corresponding leaky wave. In Section VI the signal in the waveguide is represented in the form of an approximation of the phase based on tangent function. The approximation is analyzed and the parameters of FAS are estimated. The results obtained by Miklowitz–Randles approach, leaky wave approach and the analysis of the real dispersion diagram are compared.

2 A sample two-layered waveguide

Consider a waveguide in the (x, y) -plane occupying the strip $-H_1 \leq y \leq H_2$ (see Fig. 3). The layer $H_1 \leq y \leq 0$ is filled with a medium having density and speed of sound equal to ρ_1, c_1 , respectively. The layer $0 \leq y \leq H_2$ is filled with a medium with parameters ρ_2, c_2 . The wave equations in the media are as follows:

$$c_j^2(\partial_x^2 + \partial_y^2)u_j = \ddot{u}_j, \quad (1)$$

where $u_j(x, y, t)$, $j = 1, 2$ are the field variables (say, acoustical potentials), notation \ddot{u}_j stands for the second time derivative.

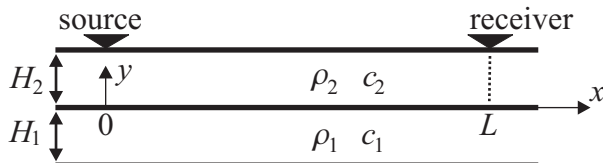


Fig. 2: Geometry of a model waveguide

The boundary conditions are as follows. The surface $y = -H_1$ is rigid (Neumann):

$$\partial_y u_1(x, -H_1, t) = 0. \quad (2)$$

On the interface $y = 0$ the pressure and the normal velocity are continuous:

$$\rho_1 u_1(x, 0, t) = \rho_2 u_2(x, 0, t), \quad \partial_y u_1(x, 0, t) = \partial_y u_2(x, 0, t). \quad (3)$$

The surface $y = H_2$ is also rigid, but a point source is located at the point $(0, H_2)$:

$$\partial_y u_2(x, H_2, t) = \delta(x)f(t), \quad (4)$$

where δ is the Dirac delta-function, $f(t)$ is the time shape of the probe pulse. The observation point is located at (L, H_2) , i. e. the function $u_2(L, H_2, t)$ is recorded.

The problem of finding the signal on the receiver is quite standard and it can be solved easily. Namely, perform the 2D Fourier transform of u_j in the domain of time and frequency:

$$\tilde{U}_j(k, y, \omega) = \int_{-\infty}^{\infty} \int_{-\infty}^{\infty} u_j(x, y, t) e^{i\omega t - ikx} dx dt. \quad (5)$$

Get a 1D problem for $\tilde{U}_j(k, y, \omega)$ as functions of y . These functions should obey the equations

$$(\partial_y^2 + \alpha_j^2) \tilde{U}_1(k, y, \omega) = 0, \quad \alpha_j = \alpha_j(k, \omega) = \sqrt{\frac{\omega^2}{c_j^2} - k^2}. \quad (6)$$

The following boundary conditions should be valid:

$$\partial_y \tilde{U}_1(k, 0, \omega) = \partial_y \tilde{U}_2(k, 0, \omega), \quad \rho_1 \tilde{U}_1(k, 0, \omega) = \rho_2 \tilde{U}_2(k, 0, \omega), \quad (7)$$

$$\partial_y \tilde{U}_1(k, -H_1, \omega) = 0, \quad \partial_y \tilde{U}_2(k, H_2, \omega) = F(\omega), \quad (8)$$

where

$$F(\omega) = \int_{-\infty}^{\infty} f(t) e^{i\omega t} dt \quad (9)$$

The solution of (6), (8), (7) can be found:

$$\tilde{U}_2(k, H_2, \omega) = F(\omega) \frac{M(k, \omega)}{N(k, \omega)}, \quad (10)$$

$$M(k, \omega) = \frac{\alpha_1}{\alpha_2} \sin(\alpha_1 H_1) \sin(\alpha_2 H_2) - \frac{\rho_1}{\rho_2} \cos(\alpha_1 H_1) \cos(\alpha_2 H_2), \quad (11)$$

$$N(k, \omega) = \alpha_2 \frac{\rho_1}{\rho_2} \cos(\alpha_1 H_1) \sin(\alpha_2 H_2) + \alpha_1 \sin(\alpha_1 H_1) \cos(\alpha_2 H_2). \quad (12)$$

The field on the receiver can be obtained by inverting the Fourier transformation:

$$u_2(x, H_2, t) = \frac{1}{4\pi^2} \iint_{-\infty}^{\infty} F(\omega) \frac{M(k, \omega)}{N(k, \omega)} e^{ikx - i\omega t} dk d\omega \quad (13)$$

Formula (13) cannot be used directly, since zeros of the denominator belong to the plane of integration. The limiting absorption principle is used to change the contour of integration. Namely, for $\omega > 0$ we assume that the velocities c_j have vanishing *negative* imaginary parts, while for $\omega < 0$ the velocities c_j have vanishing *positive* imaginary parts. Due to this, for each ω the zeros of N in the complex k -plane become displaced from the real axis.

The dispersion diagram represents the zeros of $N(k, \omega)$ (for real c_j), i. e. the dispersion equation is

$$\frac{\alpha_1 \tan(\alpha_1 H_1)}{\alpha_2 \tan(\alpha_2 H_2)} = -\frac{\rho_1}{\rho_2}. \quad (14)$$

The roots of (14) are curves in the (k, ω) plane, each point of which corresponds to a wave freely propagating in the waveguide and having x - and t -dependence of the form $\exp\{i(kx - \omega t)\}$.

3 Numerical demonstration of FAS

The following parameters have been selected for a numerical demonstration of FAS presence: $H_1 = 1$, $H_2 = 0.4$, $c_1 = 1$, $c_2 = 5$, $\rho_1 = \rho_2 = 1$. Dimensionless values are used in the computations, since no particular physical medium

is under the investigation. The values plotted in the graphs are, therefore, also dimensionless. The dispersion diagram for this waveguide is shown in Fig. 1. The fastest pseudo-branch is shown in the figure as a dashed line. The pseudo-branch is composed of parts of real branches of the diagram. One can see that for the selected parameters the pseudo-branch is quite loose, i. e. the gaps between its parts are quite wide.

For the demonstration we are using the probe pulse $f(t)$ having the spectrum corresponding to the pseudo-branch. Namely, we are using the region $20 < \omega < 40$. In this region the group velocities of the guided waves are smaller than 2.7. In the demonstration we are going to show the presence of a pulse whose velocity is approximately equal to the inverse of the slope of the dashed line. This velocity is close to 4. Thus, the velocity of the FAS is considerably higher than that of any of the guided waves.

The shape of the pulse $f(t)$ is shown in Fig. 3, left. The spectrum of this pulse is shown in Fig. 3, right. One can see that $f(t)$ is a radio pulse centered around $t = 0$. The central circular frequency is about $\omega_0 = 28$.

The results of the computations made by formula (13) for $L = 10, 20, 30$ are shown in Fig. 4, Fig. 5, Fig. 6, respectively. The field at the receiver, i. e. $u_2(L, H_2, t)$, is plotted. One can see that in all graphs there exists a small pulse, which can be interpreted as FAS.

Parameters of FAS approximately determined from these graphs are given in Table 1. ToF is the “time of flight”, i. e. the travel time of FAS. One can see that the velocity of the pulse is more than 4, and the amplitude decay is

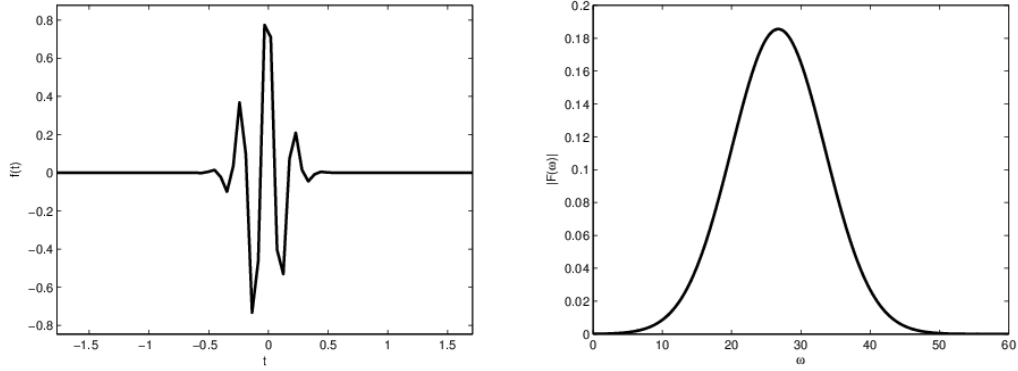


Fig. 3: Probing pulse $f(t)$ (left) and its spectrum (right)

close to exponential. Such a behavior is typical for FAS. The aim of the rest of the paper will be to estimate the group velocity of the FAS pulse $v_{g,\text{FAS}}$ and the decay parameter κ . The decay parameter is the coefficient in the exponential dependence of the amplitude vs L :

$$\text{Amplitude} \sim e^{-\kappa L}.$$

L	ToF	Amplitude
10	2.5	$1.8 \cdot 10^{-2}$
20	4.8	$2.5 \cdot 10^{-3}$
30	6.9	$5.0 \cdot 10^{-4}$

Table 1: Parameters of the FAS

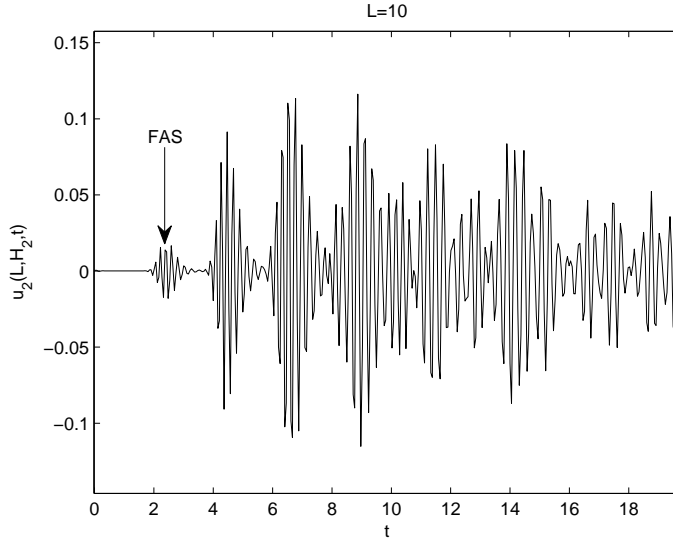


Fig. 4: Output pulse for $L = 10$

4 An approach by Miklowitz and Randles

Here we are describing a modified version of the approach introduced by Randles and Miklowitz in [3]. The modifications (compared with [3]) are as follows: the change of variables made by the authors is omitted, and the variation of the contour of integration is performed locally in the region of interest with respect to temporal and spatial frequencies.

Let function $f(t)$ be real. Consider the function

$$u'_2(x, H_2, t) = \frac{1}{4\pi^2} \int_0^{\infty} \int_{-\infty}^{\infty} F(\omega) \frac{M(k, \omega)}{N(k, \omega)} e^{ikx - i\omega t} dk d\omega, \quad (15)$$

i. e. exclude the negative values of ω . Obviously,

$$u_2(x, H_2, t) = 2\text{Re}[u'_2(x, H_2, t)]. \quad (16)$$

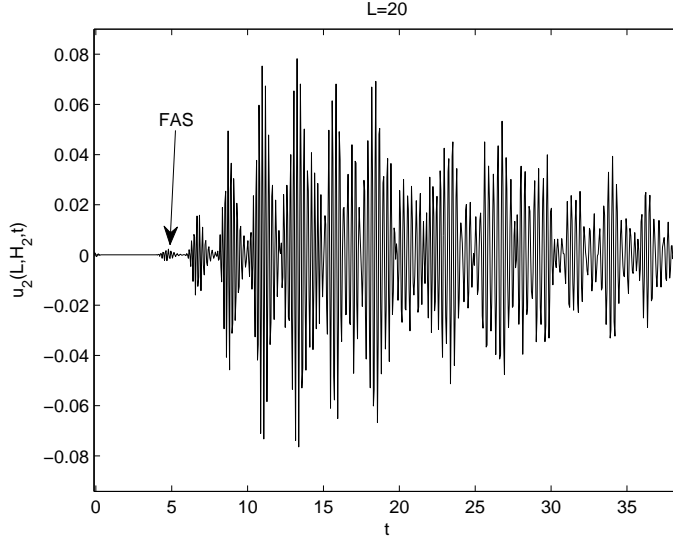


Fig. 5: Output pulse for $L = 20$

For each fixed positive ω find the roots of (14) by solving it as an equation with respect to k . Denote by $\xi_n(\omega)$ the roots having positive imaginary part or zero imaginary and positive real part. These roots correspond to waveguide modes traveling in the positive x -direction or decaying in this direction. Note that for for each $\omega > 0$ and for $x > 0$ the integral with respect to k in (15) can be considered as a contour integral, and the contour (the real axis) can be closed in the upper half-plane. The integrand is a meromorphic function in the upper half-plane, so the integral can be converted into a sum of residual terms:

$$u'_2(x, H_2, t) = \frac{i}{2\pi} \int_0^\infty F(\omega) \sum_n \frac{M(\xi_n(\omega), \omega)}{N'(\xi_n(\omega), \omega)} \exp\{i\xi_n(\omega)x - i\omega t\} d\omega, \quad (17)$$

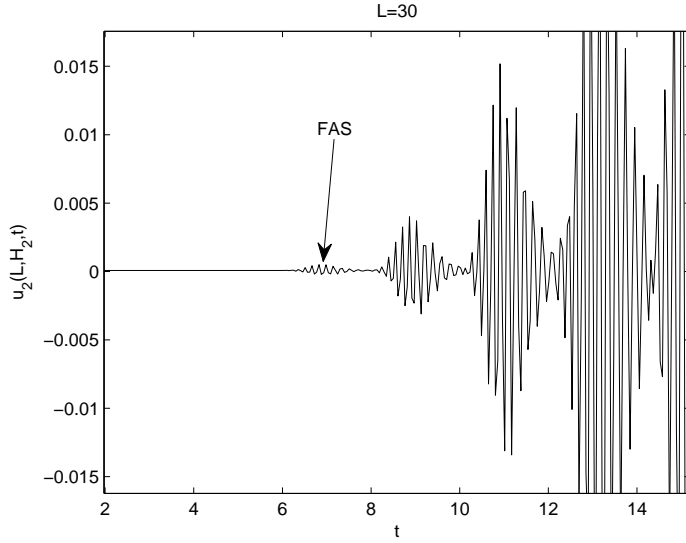


Fig. 6: Output pulse for $L = 30$

where

$$N'(k, \omega) = \partial_k N(k, \omega). \quad (18)$$

Indeed, (17) is a standard expansion of the wave field in the waveguide as a sum of waveguide modes.

For large t and x (i. e. in the far field) expansion (17) provides a comprehensive description of the wave field. Namely, each branch of the dispersion diagram with real ξ corresponds to a modal pulse, and the velocities of the modal pulses are provided by the group velocities of the branches. The branches with imaginary ξ form the near field.

For moderate t and x , however, some transient processes can occur in the waveguide. The most interesting example of such transient processes is

the FAS demonstrated in the previous section. In the transient region the standard analysis of the real dispersion diagram cannot be performed for two reasons:

- a) The modal pulses correspond to rather long fragments of the branches, on which one cannot approximate the branch by taking just its slope and curvature.
- b) Numerous branches participate in formation of a single pulse.

It was a brilliant idea of Miklowitz and Randles that one can simplify the consideration by deforming the contour of integration of (17) into the complex domain of ω . After passing some branch points the structure of the (complexified) dispersion diagram become simpler, and each transient process becomes attributed to a single branch of it. Let us illustrate this approach on the example of the FAS. As we assume, the FAS demonstrated above corresponds to a fragment of the pseudo-branch shown in Fig. 1.

Let ω be a complex variable. Continue functions ξ_n from the real axis to the complex plane. Consider $\xi_n(\omega)$ as branches of a single analytical multivalued function $\xi(\omega)$. This function, obviously, has an infinite number of sheets. Its analyticity follows from standard theorems applied to equation (14). Function $\xi(\omega)$ is defined on its Riemann surface. Practically, the continuation of ξ_n is obtained by numerical solving of equation (14) with respect to k for complex ω .

Explore a fragment of the Riemann surface. The area under investigation is shown in Fig. 7a. We are interested in behavior of the branches corre-

sponding to the real curves labeled by numbers 9–13 in Fig. 1. The fragment of the Riemann surface is shown in Fig. 7a. Small circles denote the branch points. All branch points are of order 2, i. e. they connect two sheets of the surface. The branch points form three groups: the points belonging to the real axis, the points above the real axis, and the points below the real axis.

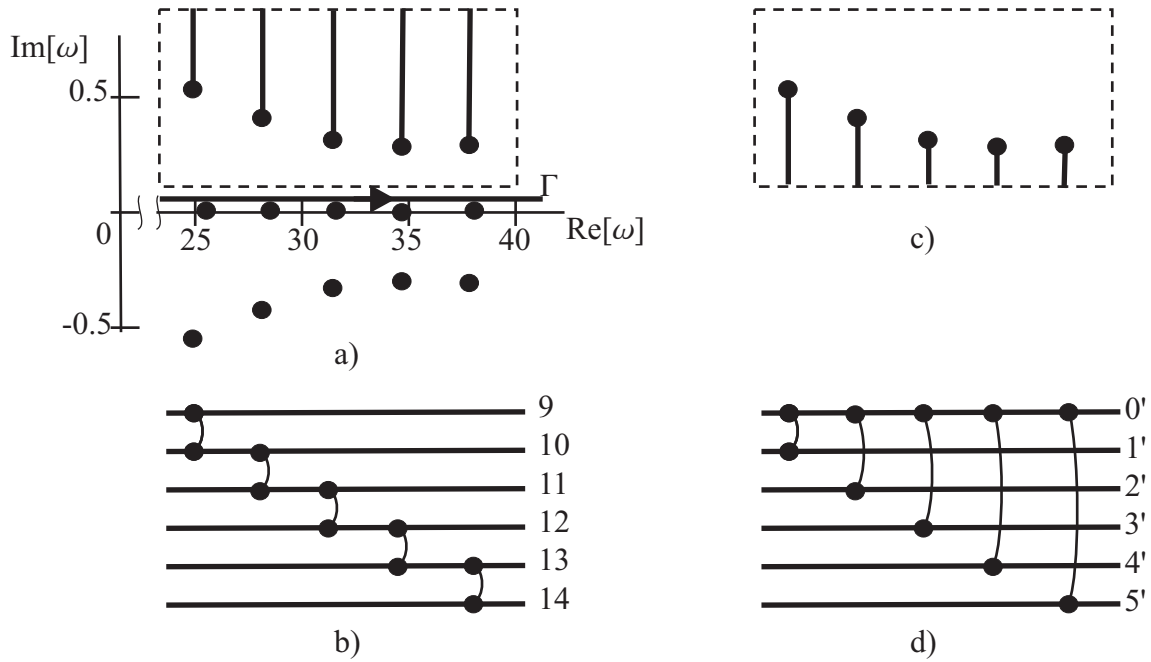


Fig. 7: Branch points on a fragment of the Riemann surface of $\xi(\omega)$

The points on the real axis correspond to the cut-off points of the waveguide modes, i. e. these branch points connect propagating branches with evanescent branches.

The branch points above the real axis play an important role. They transform a pseudo-branch into a leaky wave branch. Consider the area

of the Riemann surface bounded by a dashed rectangle in Fig 7a. Cut the fragments of the sheets lying in this area by drawing the cuts from the branch points to the top side of the rectangle (the cuts are shown by bold lines). The scheme of the Riemann surface is shown in Fig 7b. The indices of the sheets correspond to the branches of the dispersion diagram in Fig 1.

This scheme reflects the structure of the pseudo-branch, namely, the sheets are linked sequentially. Each sheet is linked with the previous one and with the next one. The same surface can be cut in a different way. Make the cuts going from the branch points to the bottom side of the rectangle. (see Fig. 7c). As the result, get the surface having scheme shown in Fig. 7d. One can see that there is a single sheet (labeled by $0'$), to which all other sheets are linked. This sheet bears the branch of the dispersion diagram similar to the leaky wave branch described in the next section.

To illustrate the structure of the Riemann surface shown in Fig. 7d, plot several branches of $\xi(\omega)$ for ω having positive imaginary part higher than the branch points. In Fig. 8 (left) we plot the real part of the dispersion diagram for $\text{Im}[\omega] = 1$. The indices correspond to the notations of sheets in Fig 7d. One can see that the branch $0'$ has a small slope $d\xi/d\omega$ i. e. a high group velocity, and there are some other branches with smaller group velocity. In the right part of the figure we plot the imaginary part of $\xi(\omega)$ corresponding to the sheet $0'$. The imaginary part of ξ for other branches are much higher, i. e. the corresponding wave components have stronger attenuation.

Let us use the knowledge of the Riemann surface of $\xi(\omega)$ to analyze

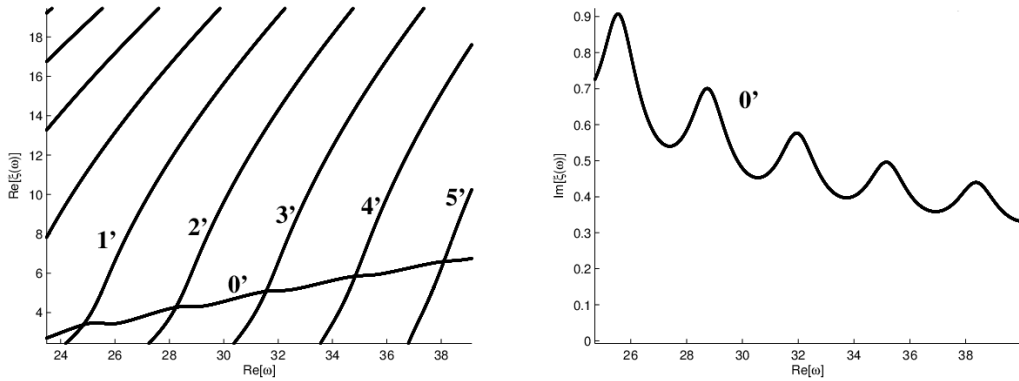


Fig. 8: A fragment of the analytical continuation of the dispersion diagram $\xi(\omega)$ for $\text{Im}[\omega] = 1$

integral (17). Rewrite this integral in the form

$$u'_2(x, H_2, t) = \frac{i}{2\pi} \int_{\Gamma} A(\omega) \exp\{i\xi(\omega)x - i\omega t\} d\omega, \quad (19)$$

where contour Γ is a sum of an infinite number of contours going from 0 to ∞ along different sheets of the Riemann surface of $\xi(\omega)$, and $A(\omega)$ is a multivalued function (all non-exponential factors of the integrand of (17)). A natural assumption can be made that $A(\omega)$ can be continued into the upper half-plane of ω , and the Riemann surface of $A(\omega)$ has the same branch points and the same topology as the Riemann surface of $\xi(\omega)$.

The idea of Miklowitz and Randles (formulated in a slightly different form and for a different type of waveguide) is to deform the contour of integration Γ shown in Fig. 7a first into the contour shown in Fig. 9a and then into the contour shown in Fig. 9b. Note that Γ is a set of contours on different sheets, and all of them are deformed simultaneously.

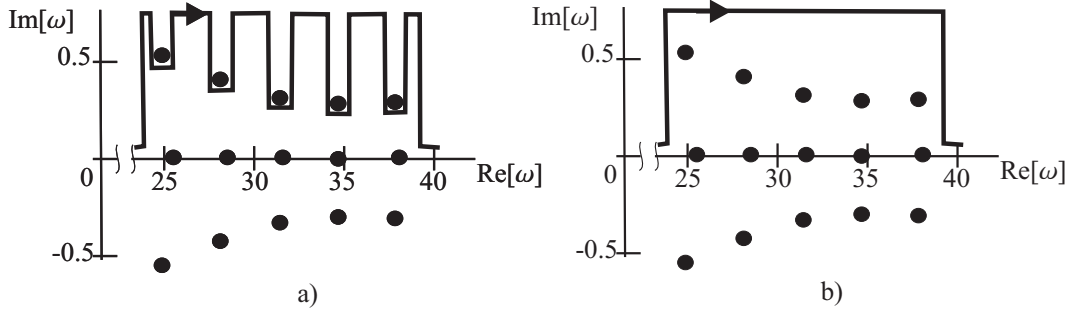


Fig. 9: Deformation of contour of integration in (19)

The change of contour of integration should be commented as follows.

- Transformation from the contour shown in Fig. 9a to the contour shown in Fig. 9b is possible since all branch points have order 2, and contour Γ is composed of contours located on all sheets. The integrals along the vertical parts encircling the branch points compensate each other.
- For some x and t such a deformation leads to an exponential decrease of the exponential factor of the integrand. Namely, let x/t be greater than any of the values $(\text{Re}[d\xi/d\omega])^{-1}$ within the area in the dashed rectangle. These values are indeed the group velocities of the branches. Then the exponential factor $\exp\{ix(\xi - i\omega t/x)\}$ decreases as $\text{Im}[\omega]$ grows, and this decrease is exponential if x is a large parameter for fixed x/t . Thus, the contour deformation can be used for finding the transient wave components that are faster than usual modal pulses.

After the deformation of the contour one gets the integral on the sheet labeled as $0'$ (describing the FAS) and many other integrals corresponding

to smaller wave components, which can be neglected. Since the behavior of the branch $0'$ is more regular than that of the initial real dispersion diagram, one can introduce the group velocity of FAS by

$$v_{\text{g,FAS}} = \left(\frac{d\xi_{0'}}{d\omega} \right)^{-1} \quad (20)$$

and define the decay parameter κ of the FAS as

$$\kappa = \text{Im}[\xi_{0'}(\omega)] - \frac{\text{Im}[\omega]}{v_{\text{g,FAS}}} \quad (21)$$

taken for $\text{Re}[\omega] = \omega_0$, which is medium for the wave train. Anyway, an exact definition of group velocity and decay is impossible, since generally FAS is a highly dispersive pulse.

The graphs shown in Fig. 8 enable one to estimate $v_{\text{g,FAS}}$ as approximately 4.0. Parameter κ varies considerably within the frequency band of the pulse (between 0.1 and 0.6). One can assume that the components of the FAS with higher frequencies has lower decay than the low-frequency components.

5 FAS as a leaky wave

To study the leaky wave we make the lower medium occupying the whole half-space $y < 0$. Let us explain why the analytical continuation of the dispersion diagram into the complex domain of ω reveals a mode whose structure is close to a leaky wave. The structure of FAS in a simplest case is shown in Fig. 10. One can see that it consists of a leading pulse traveling in the fast medium and the head wave traveling in the slow medium. The dispersive

relation for FAS is similar to that of the leaky wave if the slow medium can be substituted by a half-space, i. e. if the waveguide does not feel the lower boundary. If the analytical continuation into the complex domain of ω is made, and if $k \approx \omega/c_2$ (which is the case), then $\alpha_0 \approx 0$, while α_1 has a considerable imaginary part. The imaginary part of α_1 corresponds to transversal decay of the waves in the slow medium. This decay eliminates the influence of the lower boundary.

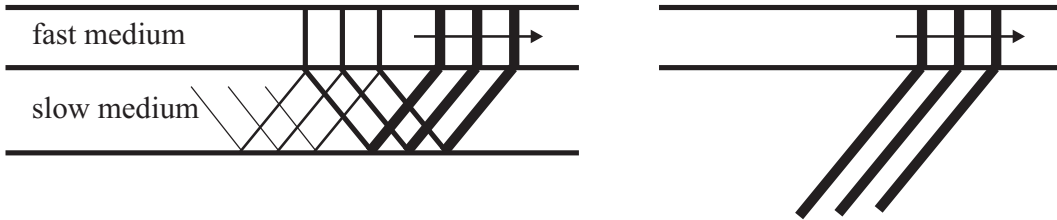


Fig. 10: Structure of FAS (left) and leaky wave (right)

The structures of the FAS and the leaky wave shown in Fig. 10 demonstrates that the leaky wave model should not work well for strongly dispersive FAS. Namely, if the FAS pulse in the upper medium starts to be wider than the distance between the beginning of the pulse and the reflection coming from the lower boundary, the leaky wave model fails to describe the wave process.

The dispersion relation for the leaky wave in our case has form

$$\frac{\rho_1 \alpha_2(\omega, \xi_L) \tan(\alpha_2(\omega, \xi_L) H_2)}{\rho_2 \alpha_1(\omega, \xi_L)} = -i \quad (22)$$

In Fig. 11 the roots of this dispersion relation are compared with analytical continuation of the dispersion diagram constructed before. Thin solid lines

correspond to the leaky wave dispersion diagram $\xi_L(\omega)$ for $\text{Im}[\omega] = 0$. Dashed lines correspond to the analytical continuation of the leaky wave dispersion diagram, namely to $\text{Im}[\omega] = 1$. The bold lines correspond to the branch $\xi_{0'}(\omega)$ found above for $\text{Im}[\omega] = 1$. The circles are related to the real dispersion diagram analysis described in the next section.

The dispersion relation $\xi_L(\omega)$ for the leaky wave can be used for estimation of the parameters of FAS in a very straightforward way. Namely, the velocity of FAS can be estimated as $\text{Re}[d\xi_L/d\omega]^{-1}$, while the decay parameter κ can be approximated as $\kappa \approx \text{Im}[\xi_L(\omega_0)]$.

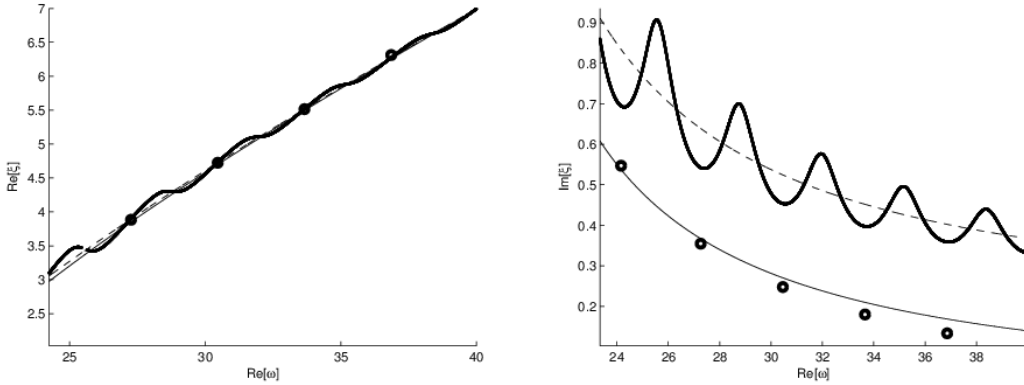


Fig. 11: Comparison of the leaky wave dispersion diagram with the branch $\xi_{0'}$ and with the estimations based on the real dispersion curve. The left side displays the real part, the right side displays the imaginary part

6 Analysis of the real dispersion diagram

In the previous sections we described two approaches to FAS. The Miklowitz–Randles approach requires a continuation of the dispersion diagram into the domain of complex ω . The leaky wave approach requires a reduced physical model that can be sometimes difficult to construct. Here we describe an alternative approach based on analysis of the real dispersion diagram. One of the benefits of this approach is that it can be used even when the only available information about the waveguide is a numerical description of the dispersion diagram. However, the concepts described above are necessary for understanding of the current approach.

Consider an approximation to $\xi(\omega)$ taken in the vicinity of the pseudo-branch:

$$\xi_a(\omega) = a \tan(\beta\omega + \gamma) + \frac{\omega}{v} + c \quad (23)$$

where a , β , γ , v , c are some parameters. Parameter β is linked to the number of real branches crossing the pseudo-branch per some unit length $\Delta\omega$. Parameter a shows how loose is the pseudo-branch.

Consider the field in vicinity of the point $(t, x = vt)$. To study the integral of the form (19) deform the contour of integration as it was described above and continue $\xi(\omega)$ into the upper half-plane of complex ω . The most important observation is that for large β

$$\tan(\beta\omega + \gamma) \rightarrow i$$

in the upper half-plane. Thus, the decay of the wave corresponding to the

pseudo-branch can be estimated as

$$\kappa \approx a. \tag{24}$$

Obviously, the velocity of the wave component associated with the pseudo-branch is equal to v .

The procedure of estimation of v and a is as follows. It is natural to assume that the pseudo-branch passes through the points of the dispersion diagram, at which the slope $d\xi/d\omega$ has local minimums (i. e. the group velocity has local maximums). Denote these points by ω_n^* . We are trying to find such parameters v and c that the linear function $\xi = \omega/v + c$ fits these points of the dispersion diagrams. Then we try find the tangent function parameters a , β and γ such that the approximation function (23) coincides with the real dispersion diagram $\xi(\omega)$ at the points $(\omega_n^*, \xi(\omega_n^*))$ and has the slope $d\xi_a(\omega_n^*)/d\omega$ at these points equal to the slope $d\xi(\omega_n^*)/d\omega$ of the dispersion diagram.

In Fig. 12 we plot a fragment the group velocities graph related to Fig. 1. The wavenumber k and the group velocity v_{gr} related to each local maximum ω_n^* are given by Table 2.

ω_n^*	24.16	27.26	30.46	33.66	36.86
$k(\omega_n^*)$	3.0	3.88	4.72	5.51	6.31
$v_{\text{gr}}(\omega_n^*)$	1.24	1.63	1.97	2.27	2.54

Table 2: Characteristics of local peaks of group velocity

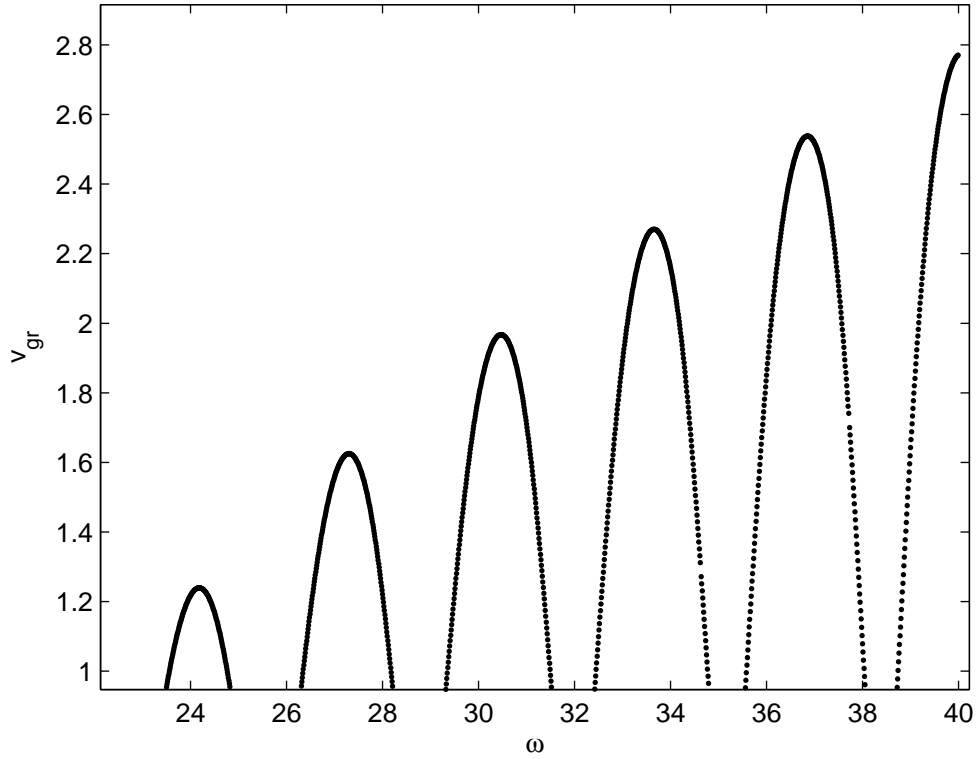


Fig. 12: Group velocities of the modes

The estimation of v is, obviously,

$$v \approx \frac{\omega_{n+1}^* - \omega_n^*}{k(\omega_{n+1}^*) - k(\omega_n^*)} \quad (25)$$

This parameter is an estimation of $v_{g,FAS}$. The estimation of β is

$$\beta \approx \frac{\pi}{\omega_{n+1}^* - \omega_n^*}. \quad (26)$$

Finally, the estimation of a is as follows:

$$a \approx \frac{1}{\beta} \left(\frac{d\xi(\omega_n^*)}{d\omega} - \frac{1}{v} \right). \quad (27)$$

Since the values of a given by (27) are different for different points ω_n^* , we come to conclusion that a in (23) is a (slow) function of ω . By (27) we obtain an estimation of a at the points ω_n^* , and after that we can, say, interpolate a between these points. As we mentioned above, function a is an estimation of the decay parameter κ .

Using the data extracted from Fig. 12 and Fig. 1 collected in Table 2, we can estimate the position of the pseudo-branch and the values of the attenuation parameters. The points related to the peaks of the group velocity are plotted in Fig 11 as small circles. One can see that the points obtained from the the real dispersion diagram are in reasonably good agreement with the dispersion curve of the leaky wave for real ω .

7 Conclusion

It is shown that FAS pulses correspond to terrace-like structures of the dispersion diagrams. These structures are called pseudo-branches in the paper. A typical form of the pseudo-branch is shown in Fig. 1. The pulse propagation velocity for FAS is the inverse of the slope of the dashed curve in Fig. 1, and it can be larger than any of the group velocities available in the considered part of the dispersion diagram.

In the paper we describe three different approaches to finding the velocity and the decay of FAS pulses. They are the Miklowitz–Randles approach based on the analytical continuation of the dispersion diagram, The leaky

wave approach and the approach based on the analysis of the pseudo-branch of the real dispersion diagram. Only the third approach is original. In the third approach one should study the local peaks of the the group velocity, i. e. find the positions of the peaks and the values of the group velocity. These parameters provide data describing the FAS. Our computations prove consistency of all three approaches.

Author is grateful to an anonymous referee who attracted his attention to the leaky wave approach.

The work is supported by the grants RFBR 14-02-00573 and Scientific Schools-283.2014.2.

References

- [1] M. Muller, P. Moilanen, E. Bossy, P. Nicholson, V. Kilappa, J. Timonen, M. Talmant, S. Cheng, and P. Laugier (2005) “Comparison of three ultrasonic axial transmission methods for bone assessment,” *Ultras. Med. Biol.* **31**, 633–642.
- [2] J. Grondin, Q. Grimal, K. Engelke, and P. Laugier (2010) “Potential of first arriving signal to assess cortical bone geomtery at the hip with QUS: a model based study,” *Ultras. Med. Biol.* **36**, 656–666.
- [3] P.W. Randles, J. Miklowitz (1971) “Modal representations for the high-frequency response of elastic plates,” *Int. J. Solids Struct.* **7**, 1031–1055.

- [4] J. Miklowitz (1978) The theory of elastic waves and waveguides, North-Holland publishing company, 618.
- [5] E. Camus, M. Talmant, G. Berger, and P. Laugier (2000) “Analysis of the axial transmission technique for the assessment of skeletal status,” Journ. Acoust. Soc. Am., **108**, 3058–3065.
- [6] R.D. Mindlin (1960) “Waves and vibrations in isotropic, elastic plates” In: Structural Mechanics. Eds J.N. Goodier and N. Hoff. Pergamon Press: New York, 199–232.
- [7] P.W. Randles (1969) Modal representations for the high-frequency response of elastic plates, Ph.D. thesis, Caltech.
- [8] L.B. Felsen, N. Marcuwitz (2001) Radiation and scattering of waves, Wiley-IEEE Press, 924.